

The Use of Glow Discharge Optical Emission Spectroscopy to Quantify Internal Carburization in Supercritical CO₂

Michael J. Lance
Senior R&D Staff Member
Oak Ridge National Laboratory
Oak Ridge, TN 37831-6068
lancem@ornl.gov

Donovan N. Leonard
R&D Staff Member
Oak Ridge National Laboratory
Oak Ridge, TN 37831-6064
leonarddn@ornl.gov

Bruce A. Pint
Group Leader
Oak Ridge National Laboratory
Oak Ridge, TN 37831-6156
pintba@ornl.gov



Michael J. Lance is a Senior Research and Development Staff Member in Oak Ridge National Laboratory's Materials Science and Technology Division. He received a B.S. in 1992 from Alfred University and an M.S. and PhD from Rutgers University in 1998 in Ceramic Science and Technology. He joined Oak Ridge National Laboratory as a staff member in 1998 and has been active in several research areas including emissions control technologies for diesel engines, high-temperature oxidation and heat exchanger fouling.



Donovan N. Leonard is a Senior Technical Staff Member in the Materials Science & Technology Division at Oak Ridge National Laboratory. He received his Ph.D. in Materials Science & Engineering from North Carolina State University in 2002 and joined ORNL in 2007. Currently his research involves applying advanced microscopy and microanalysis methods to energy related materials at length scales from the atomic level to the macro scale. More specifically, aberration corrected STEM/EELS of quantum materials in addition to EPMA/WDS, EBSD and EDS analysis of materials for fossil, fusion and solar applications.



Bruce A. Pint is the Group Leader of the Corrosion Science & Technology Group in the Materials Science & Technology Division at ORNL. He received his Ph.D. from M.I.T. in Ceramic Science and Engineering in 1992 and has been at ORNL since 1994. Dr. Pint is the principal investigator for numerous R&D projects including corrosion issues in fossil energy, nuclear energy, fusion energy and combined heat and power systems. His research covers compatibility, lifetime predictions, environmental effects and coatings in all types of power generation. He is a Fellow of NACE International and ASM International.

ABSTRACT

To analyze the compatibility of structural alloys in supercritical CO₂ (sCO₂), techniques are needed to quantify any potential alloy degradation. A specific concern for sCO₂ environments is the ingress of C into the alloy, which has been observed for more than 50 years in both Fe- and Ni-based alloys. Recently, Glow Discharge Optical Emission Spectroscopy (GDOES) has been increasingly used to measure the concentration of light elements, like C, as a function of depth. As part of a current effort to model the lifetime of structural alloys in sCO₂ at 700-800 °C, several Fe- and Ni-base alloy specimens were

analyzed after 1,000-5,000 h exposure in 1 and 300 bar CO₂. In general, the specimens exposed at 750°C showed little or no C ingress. This may be due to the dense external Cr₂O₃ scale formed on these alloys, which inhibited C transport. At lower temperatures, 550-700 °C, C ingress was detected in both Fe- and Ni-base alloys.

INTRODUCTION

Supercritical CO₂ (sCO₂) is being considered as a working fluid for a range of power generation applications [1-4]. The key issue for oxidation in CO₂ is the potential for C ingress through the oxide scale that forms on the surface of structural alloys, which was identified more than 50 years ago [5-9]. As the activity of oxygen drops across the scale from the gas interface to equilibrium (e.g. Cr/Cr₂O₃) at the metal interface, there is a corresponding increase in the carbon activity. Thus, for a lifetime modeling effort [10-12], a key focus was to measure the amount of C ingress as a function of time and temperature in order to predict long-term behavior (e.g. a 30-year lifetime for a concentrated solar power application corresponds to ~100,000 h of operating time).

One experimental tool able to measure carbon alongside other elements as a function of depth is radio frequency glow discharge optical emission spectroscopy (GDOES) [13]. The technique is based upon the sputtering of the surface with an electric field induced radio frequency (r.f.) plasma (or glow discharge) using low pressure Ar gas. The argon collides with the surface thereby sputtering atoms off the sample surface that then enter the plasma where they are excited by colliding with high-energy electrons and gas atoms. These excited atoms de-excite by optical emission releasing photons with energies that are characteristic of the atom. The optical emission is dispersed with a grating and measured with photomultiplier tubes (PMTs). The measured intensities are directly proportional to the number of sputtered atoms for each element. With high dynamic range PMTs, elemental concentrations can be measured from parts-per-million (ppm) levels up to 100%. Over 40 elements can be measured in parallel with commercially-available instruments. Also, GDOES can acquire depth profiles up to ~200 μm deep in less than one hour making it ideally suited for analyzing corroded surfaces and depletion zones. It must be stressed, however, that the depth profile is averaged across a circular area 2 – 7 mm in diameter and GDOES cannot generate two-dimensions maps of elemental composition from a cross-section or surface as is routinely done with electron probe microanalysis (EPMA) and energy dispersive x-ray spectroscopy (EDS).

GDOES has been used to measure concentration depth profiles on corrosion samples for many years with focus on tracking the presence of light elements which GDOES is able to detect with higher sensitivity than x-ray techniques (i.e., EPMA and EDS). For instance, Jalowicka, et al., used GDOES to measure B and N depletion in a Ni-base alloy down to ~0.01 at% [14]. GDOES has also been used to measure Li in graphite anodes [15], S distributions in commercial Ni-base alloys following exposure to SO₂ [16] and in a Fe-base alloy [17], and O uptake in air plasma sprayed MCrAlY coatings [18]. GDOES is particularly useful in the detection of H, D (deuterium) and He since these atoms have no inner shell electrons and therefore cannot be directly detected with x-ray techniques. Dumerval et al. used this feature of GDOES to detect hydrogen adsorption in stainless steel 316L following exposure to environments present in pressurized water reactors [19]. Of great interest to the fusion energy community is the unique ability of GDOES to differentiate D₂ from He, which have nearly identical atomic masses and so cannot be easily separated with mass spectrometry [20]. More recently researchers have begun to use GDOES to measure C concentration profiles in alloys exposed to CO₂ and sCO₂ environments [21-30] where the detection limit approaches 10 ppm C. This paper presents preliminary results on Ni and Fe-base alloys exposed to sCO₂ collected using a new GDOES system at Oak Ridge National Laboratory.

EXPERIMENTAL PROCEDURE

The chemical compositions of the structural alloys measured by an outside lab using inductively coupled plasma optical emission (ICP-OE) and combustion analysis for C and O are listed in Table 1. Coupons with dimensions of ~10 x 20 x 1.5 mm were polished to a 600-grit finish using SiC paper and ultrasonically cleaned in acetone and methanol prior to exposure. For the 500-h cycles in 200 or 300 bar CO₂, the exposures were conducted in an autoclave fabricated from alloy 282. The vertically-oriented autoclave

(~266 mm x 83 mm inner diameter) was operated inside a three-zone furnace with an alloy 282 sample rack that sat on the bottom of the autoclave. The fluid flow rate was ~2 ml/min. The specimens were slowly heated to temperature over several hours (~2 °C/min) in sCO₂, held at temperature ±2 °C and then cooled in sCO₂ to room temperature by lowering the furnace and using a cooling fan on the autoclave. Additional details of the system have been provided elsewhere [31, 32]. For the 500-h cycles at 1 atm CO₂, the coupons were placed in an alumina boat in an alumina reaction tube with end caps. The specimens were heated in argon to 750 °C over 4 h to minimize oxidation of the sample prior to exposure to CO₂, held for 500 h in CO₂ and cooled in argon to room temperature. Gas flow rates were ~300 cc/min. For 10-h cycles, samples were hung from alumina rods with platinum wire and exposed in automated cyclic rigs [33] for 10 h in the hot zone followed by 10 min cooling in laboratory air to <30 °C after being automatically pulled from the furnace. Exposures at 700, 750 and 800 °C were conducted in industrial grade (IG) CO₂ at 1 bar, with <60 ppm O₂ and <32 ppm H₂O. Gas flow rates were ~100 cc/min or ~0.1 cm/s flow rate.

For all the experiments, the specimens were weighed using a Mettler Toledo XP205 balance with an accuracy of ~±0.04 mg or 0.01 mg/cm². Mass change was measured every 500-h cycle or every 160 h in the 10-h cyclic tests. After exposure, samples were copper plated before being sectioned and mounted metallographically for light microscopy.

Table 1. Alloy compositions in atomic percentage. “λ” refers to the emission line used for GDOES.

Alloy	Fe	Ni	Cr	Co	Mo	Al	Ti	Si
740	0.11	47.54	24.47	19.64	0.18	2.89	1.62	0.30
282	0.17	56.04	21.74	10.36	5.16	3.49	2.63	0.07
SN25	43.30	24.55	24.39	1.43	0.12	0.053	0.028	0.31
625	4.22	61.67	24.85	0.13	5.50	0.27	0.28	0.33
λ (nm)	373.49	352.45	425.43	345.35	386.41	396.15	334.94	288.16
Alloy	Mn	Nb	W	Cu	V	Zr	C	O
740	0.26	0.89	0	0	0.009	0.014	0.126	0.002
282	0.021	0	0	0	0.011	0	0.283	0.003
SN25	0.54	0.29	1.07	2.68	0.059	0	0.322	0.009
625	0.17	2.19	0.02	0.084	0.022	0	0.079	0.004
λ (nm)	403.45	316.34	429.46	324.75	411.18	360.12	156.14	130.22

GDOES was performed using a Horiba GD Profiler 2 equipped with a differential interferometry profiling (DiP) system. The argon gas pressure was 850 Pa and the power was 50 W for all measurements. Prior to measurement, any air between the anode and the sample was removed by flushing with three high/low Ar pressure cycles followed by one very high Ar pressure flush. The background for each element was measured for 5 seconds prior to sputtering and the wavelength of the emission lines used for GDOES for each element are listed in Table 1. Measurements were made every 0.1 s and collection proceeded for at least 480 s which resulted in a sputtered dimple at least 50 μm deep. The anode diameter was 4 mm which defines the size of the region measured across the sample surface. Figure 1a shows the raw intensity data in log scale measured in PMT voltage collected from alloy 282 that had been exposed to 300 bar of CO₂ at 700 °C for four 500-h cycles. Collecting for 480 s was long enough so that the intensities reached a plateau which shows that the alloy bulk was reached by the end of the acquisition. The C intensity took longer to stabilize which is due to infiltration of C during the exposure to CO₂ and will be discussed below. The O intensity is still declining at the end of the test which is likely caused by some oxide scale around the edge of the crater being sputtered throughout the entire test and does not indicate the presence of O deep in the alloy. This low O intensity will not significantly alter the determination of composition below the oxide scale.

Figure 1b shows the depth profile determined using the differential interferometry profiling (DiP) system which is measured by directing one laser beam (λ = 633 nm) on to the intact surface and a second on to the center of the sputtered crater. Interference from the two reflected beams are compared and used to measure the sputtered depth during the acquisition. Unfortunately, since the oxide scale is translucent,

the DiP did not function properly to enable depth to be measured through the oxide scale. This can be seen in Figure 1b which also shows the intensity of O which is high during the first 30 s during sputtering of the scale. The DiP signal only starts to register a change in depth after the oxide scale has been removed. Below the oxide scale, the measured sputter rate was very constant at 8.0 $\mu\text{m}/\text{min}$. The sputter rate through the oxide was ~ 2 times slower than through the alloy.

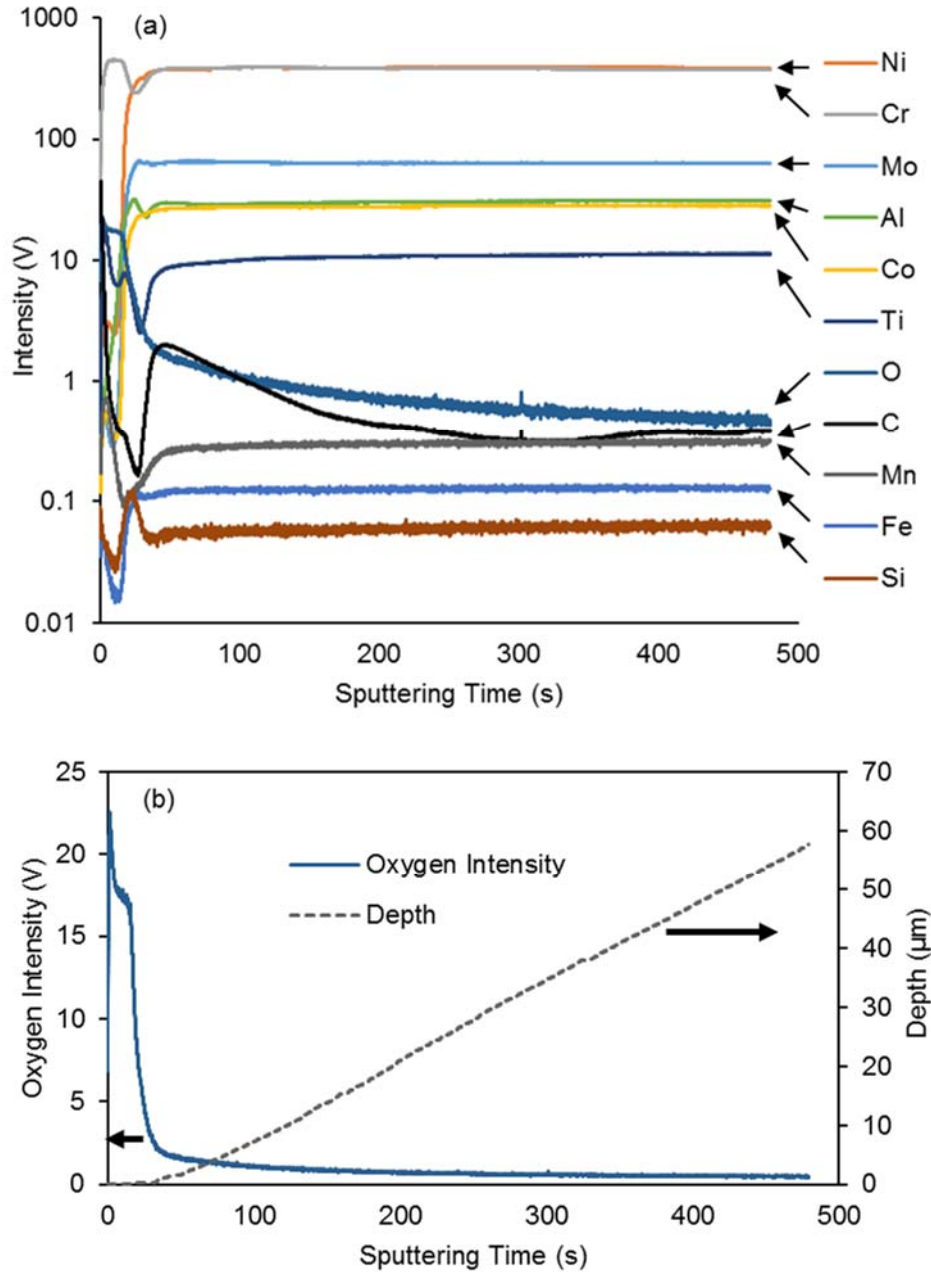


Figure 1. (a) GDOES intensity profile in log scale versus sputtering time for 282 exposed to 300 bar of CO_2 at 700 $^\circ\text{C}$ for four 500-h cycles, and (b) the depth profile collected with DiP alongside the oxygen intensity profile.

Figure 2a shows the final dimple height map after sputtering the 282 sample from Figure 1 measured

using a Keyence VR-3000 optical profilometer. Also shown in Figure 2b is a line profile across the dimple. The final dimple depth was 64 μm compared to 58 μm estimated by the DiP system (Figure 1b). The upper left corner of Figure 3 shows a secondary electron image of the scale cross section collected using a Hitachi 3400 scanning electron microscope (SEM). The 6 μm difference between the actual dimple depth and that estimated by the DiP system is about equal to the oxide scale thickness including the internal oxidation (Figure 3) which shows again that the DiP system excludes the translucent oxide scale from its depth measurement. Also measured in Figure 2b is the average roughness (R_a) of the sputtered surface which was 2.9 μm . This is the effective depth resolution of the technique under these operating conditions.

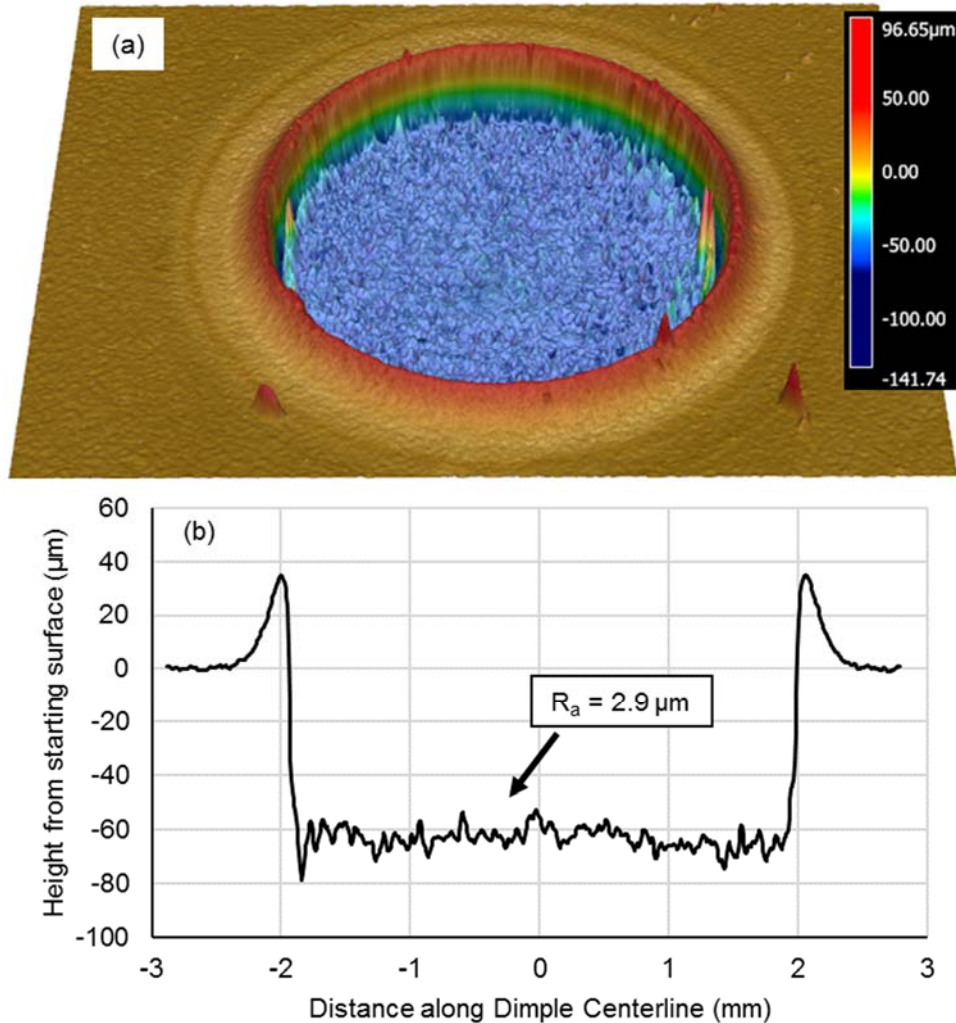


Figure 2. (a) Sputtered dimple after GDOES measurement and (b) a line profile across the dimple from the sample measured in Figure 1.

Determination of the concentration profiles from the intensity data in Figure 1a was performed following the procedure described by Nowak [34] which follows on the earlier work of Quadackers et al. [35] and Pfeiffer, et al. [36] for calibrating secondary neutrals mass spectrometry (SNMS). This procedure calibrates the intensities using either an unexposed alloy of known composition or by sputtering deep enough so that the base alloy below the depletion zone is reached which is the approach taken here. The first step is to calculate sensitivity factors for each element by dividing the known concentration of the element (c_x) in the base alloy (Table 1) by the average light intensity (I_x) during the final minute of sputtering (after the intensity has plateaued) for that element. Each sensitivity factor is then normalized to the

sensitivity factor for the base element which is Ni for alloy 282, resulting in a relative sensitivity factor (RSF_x) using the following equation:

$$RSF_x = \frac{C_x}{I_x} / \left(\frac{C_{Ni}}{I_{Ni}} \right). \quad (1)$$

The RSF for oxygen was estimated by averaging light intensity for O and Cr in a region of the scale that is composed almost entirely of Cr₂O₃ using the equation:

$$RSF_O = \left(\frac{I_{Cr} * RSF_{Cr}}{I_O} \right) \left(\frac{3}{2} \right). \quad (2)$$

Concentration for each element (c_x) is then calculated in atomic percentage using the following equation:

$$C_x = \frac{I_x * RSF_x}{\left(\sum_{i=1}^n I_i * RSF_i \right)}. \quad (3)$$

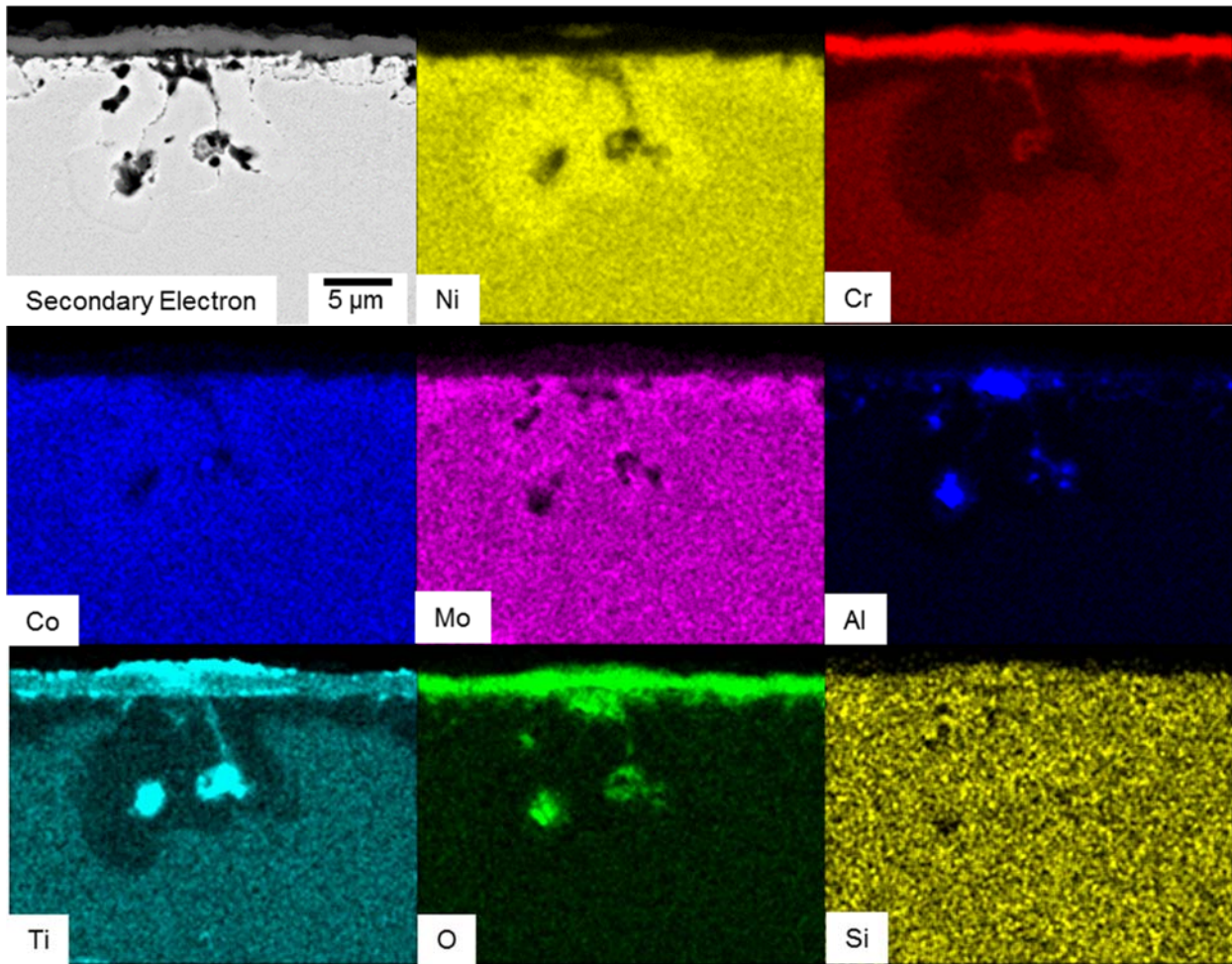


Figure 3. Secondary electron image of the oxide scale and depletion zone of 282 after exposure to 300 bar of CO₂ at 700 °C for four 500-h cycles (upper left). EDS elemental maps of Ni, Cr, Co, Mo, Al, Ti, and O and Si are also shown.

RESULTS AND DISCUSSION

Figure 4 shows the concentration profiles calculated from the intensities in Figure 1a using the procedure described above. The sputtering time was converted to depth from the oxide/metal interface using the DiP data from Figure 1b. The concentration within the oxide scale is shown versus sputtering time since the DiP technique could not measure depth in the oxide as explained above.

The oxide scale in Figure 4 is primarily Cr_2O_3 . This corresponds well to the elemental maps of the cross-section of this scale shown in Figure 3. Ti enriches the scale on the outer surface and at the oxide/metal interface as has been previously observed on alloy 282 and can be seen in both Figures 3 & 4. As the oxygen level drops near the metal, the Al concentration increases in Figure 4 which indicates the internal oxidation region seen in Figure 3. The carbon content is highest near the outer surface of the scale which is likely due to surface contamination and not from CO_2 infiltration into the scale since it occurred even on unexposed samples. The C and Cr concentration both dip below the bulk concentration right below the oxide scale which shows the consumption of chromium carbides during exposure. The decrease in Cr content beneath the Cr_2O_3 scale can also be seen in the Cr map from Figure 3. From Figure 4, about 2 μm below the metal/oxide interface, the carbon concentration increases to 1.5 at% and then starts to fall deeper into the alloy. This is clear evidence of carburization of the alloy from exposure to sCO_2 .

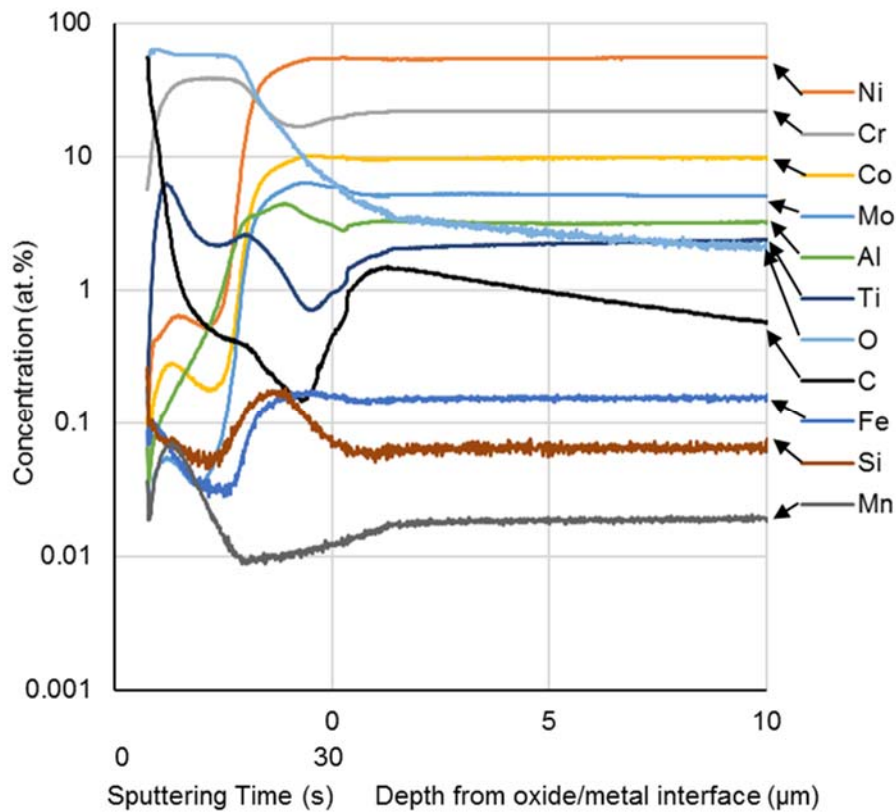


Figure 4. Concentration depth profiles calculated from intensities in Figure 1a and DiP measurements in Figure 1b. The sample was 282 exposed to 300 bar of CO_2 at 700 °C for four 500-h cycles.

Electron probe microanalysis (EPMA) maps of C, Cr and O collected from the same 282 sample measured by GDOES in Figure 4 are shown in Figure 5. EPMA utilizes wavelength dispersive spectroscopy (WDS) which is at least an order of magnitude more sensitive to carbon than EDS and so provides a better test of the sensitivity of GDOES. Spectra were collected using a JEOL Model 8200. The O map and the secondary electron image in Figure 5 both show that the oxide scale is at the top of all the maps. Just as in Figure 4 as measured with GDOES, a decline in both Cr and C directly below the oxide scale is observed

with EPMA. Further below this depleted zone, the carbon intensity rises slightly which compares well to the increase observed with GDOES in Figure 4.

Additionally, the elemental concentration was measured using EPMA on the cross-sectioned sample in Figure 5 along a line extending perpendicular to the oxide scale surface using 0.5 μm steps. The C profile from this measurement is shown in Figure 6 along with the C concentration measured on the exposed 282 sample using GDOES. The x-axis for the EPMA measurement was converted from distance to GDOES sputtering time using the sputtering rate mentioned above. The two measured C concentration profiles are similarly shaped with the C concentration measured with EPMA about 30% higher than the GDOES measurement. Since GDOES collects data across a 4-mm diameter spot, the analytical volume is orders of magnitude larger than that of EPMA and so the GDOES measurement will be more accurate with less noise. Also, despite this sample exhibiting one of the largest C concentration peaks, it was barely detected by EPMA but easily detected by GDOES. It is unlikely that EPMA could detect C concentration changes less than this whereas GDOES is sensitive to <0.1 at% changes in C concentration, as can be seen for in Figure 6 for alloy 625. Therefore, under these experimental conditions, GDOES is more sensitive to C concentration than EPMA with the caveat that data is only collected along a depth profile with GDOES as opposed to a 2-D map as with EPMA.

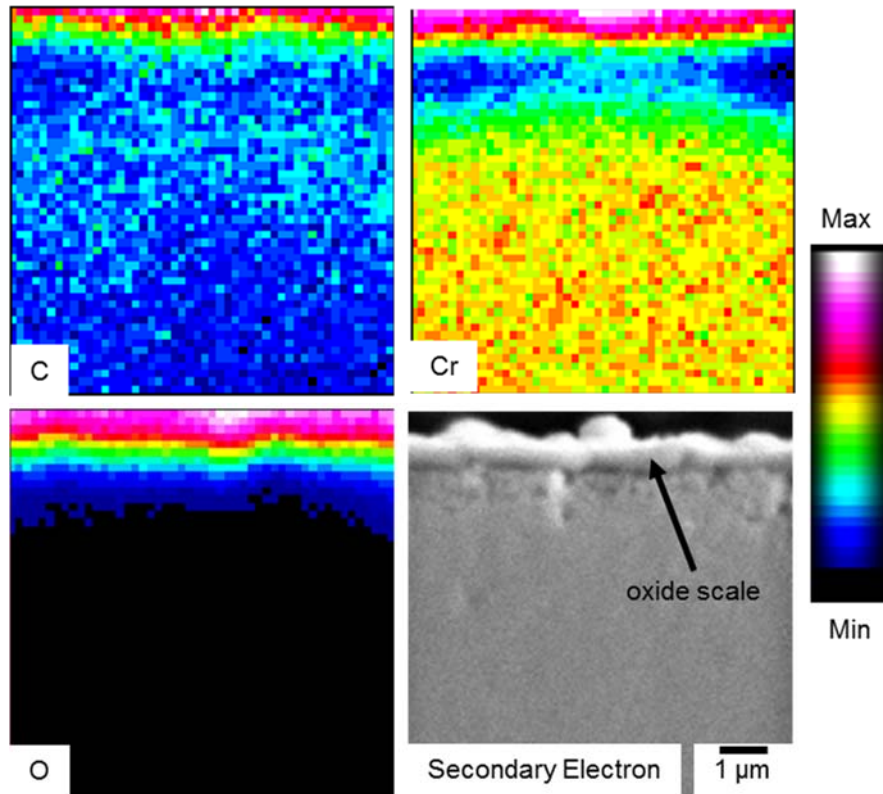


Figure 5. EPMA maps of the normalized x-ray intensities of C, Cr, and O measured adjacent to the oxide scale on sample 282 exposed to 300 bar of CO_2 at 700 $^\circ\text{C}$ for four 500-h cycles. The secondary electron image is also shown.

Figure 6 also compares the carbon concentration depth profiles for Ni-base alloys 282, 740 and 625 exposed to 300 bar of sCO_2 for four 500-h cycles at 700 $^\circ\text{C}$. No attempt was made to convert the sputtering time to depth due to the difficulties of measuring depth through the oxide as described above. All three alloys exhibited the same change in C concentration with a decrease below the oxide due to the consumption of chromium carbides followed by an increase due to carburization deeper into the alloy. The degree of carburization was highest for 282 followed by 740 and then 625.

Figure 7 shows carbon concentration profiles for the 282 alloy measured on an as received specimen, and specimens exposed at 700 °C and 750 °C both to 300 bar sCO₂ for 2000 h and 2500 h, respectively. Both specimens showed a decline in the C concentration due to loss of chromium carbides below the oxide scale but only the specimen exposed to the lower temperature showed an increase of C deeper into the alloy. One possible explanation for this is that the thicker oxide formed at the higher temperature is a better barrier to C ingress.

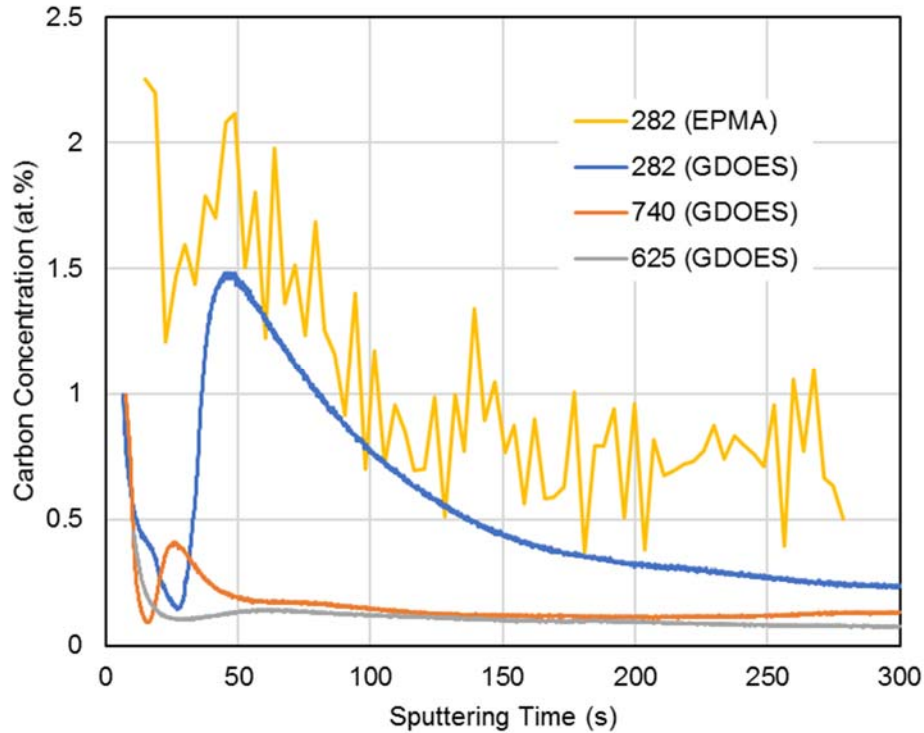


Figure 6. GDOES C concentration profiles for alloys 282, 740 and 625 exposed to 300 bar of sCO₂ for four 500-h cycles at 700 °C. The carbon concentration measured with EPMA on the 282 alloy is also shown.

In only one case did the CO₂ environment lead to accelerated oxidation. Figure 8 shows the mass gain for alloy 282 specimens at 700° and 750°C using 10-h cycles in industrial grade (IG) CO₂. All the specimens showed nearly parabolic behavior. In contrast, the Fe-based alloy 25 specimens all showed accelerated (i.e. non-parabolic) behavior. One hypothesis is that Fe-based alloys are more susceptible to C ingress because of the higher affinity of C for Fe than Ni [37]. The carbon concentration for one of the alloy 25 specimens exposed to 1 bar CO₂ at 700 °C for 4000 h (i.e. 400, 10-h cycles) is shown in Figure 9. The depletion of C is again observed below the oxide scale, consistent with the Cr depletion in this area. This result is like those shown previously for Ni-base alloys. There is a slight increase of the C concentration below the depleted zone. However, there is no indication of any large C ingress in this specimen. While the specimen was not able to maintain the formation of a thin continuous Cr₂O₃ scale, there is no strong evidence that the accelerated attack was caused by C ingress.

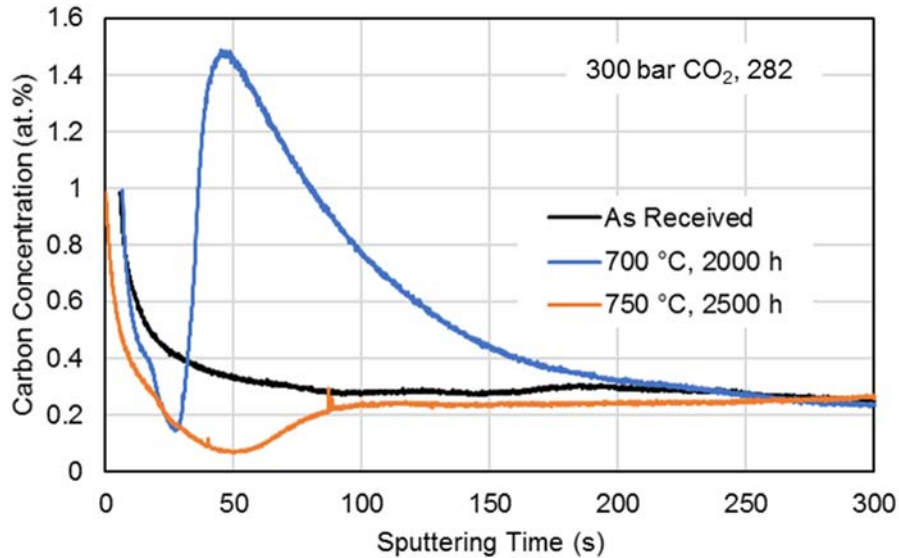


Figure 7. GDOES C concentration profiles for 282 exposed to 300 bar sCO₂ at 700 °C and 750 °C. Also shown is the as received 282 sample.

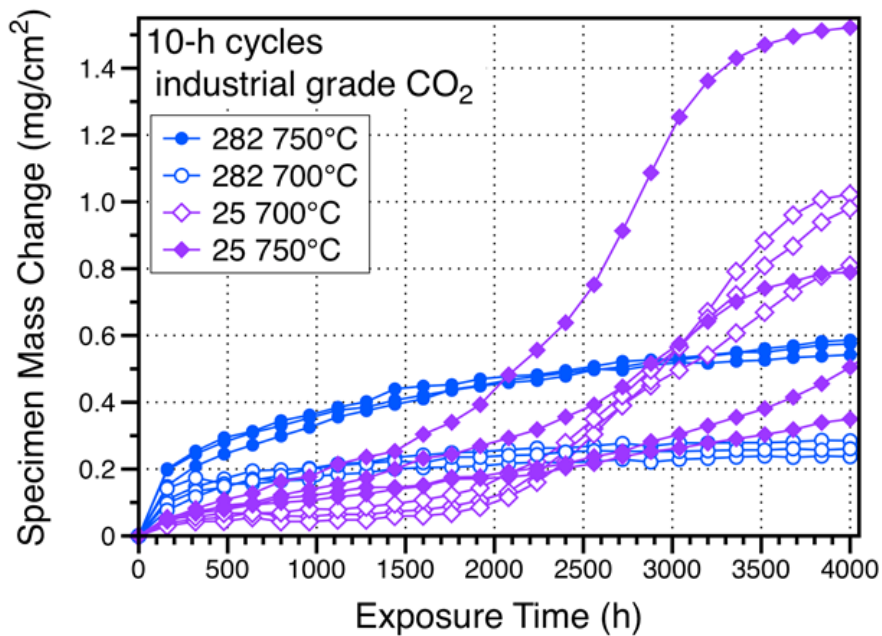


Figure 8. Specimen mass change of 282 and 25 at 700 °C and 750 °C exposed to 10-h cycles in IG CO₂. Three or four samples are shown for each exposure condition/ally.

One unusual result was observed for a set of specimens that were exposed in 200 bar research grade (RG) CO₂ at 700 °C for a round robin experiment. The mass gains for these specimens were higher than expected, which may have been caused by a dead leg (a section of piping that no longer maintains gas flow) that was not flushed between runs and may have added impurities to the system. Figure 10 shows C concentration profiles for specimens of 625 and 740 exposed for 1000 and 1500 h in this experiment. On both alloys and after both exposure times, two regions of C are observed; the first occurs within the oxide scale at ~30 s of sputtering time and the second below the oxide scale. Further characterization is needed to understand why these specimens showed a higher mass gain and how C ingress may have

affected the scale and alloy microstructure near the surface.

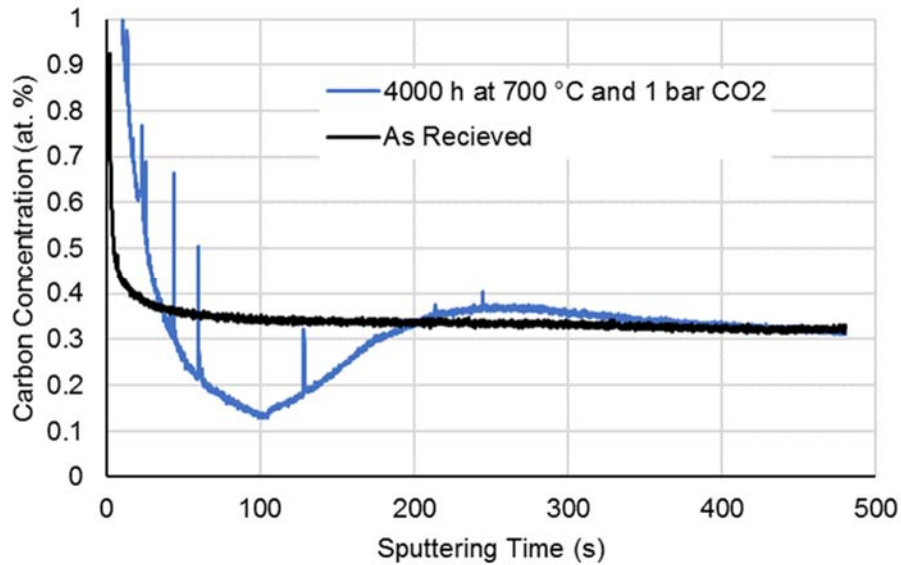


Figure 9. GDOES carbon concentration profile for alloy 25 exposed to 1 bar CO₂ at 700 °C. Also shown is C profile collected from the as-received 25 specimen.

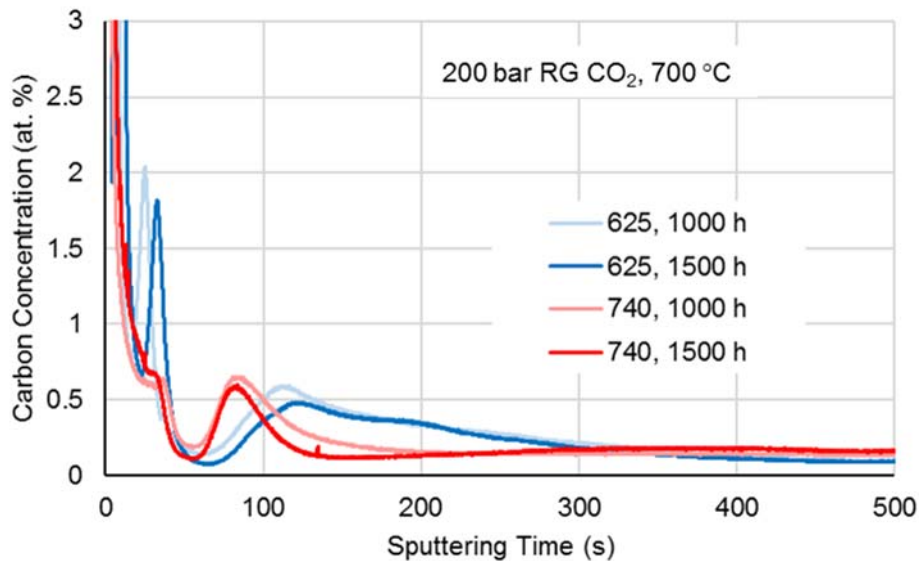


Figure 10. GDOES carbon concentration profiles for specimens of 625 and 740 exposed to 200 bar of RG CO₂ at 700 °C for 1000 and 1500 h.

CONCLUSIONS

GDOES was used to measure carbon profiles in four different alloys exposed to sCO₂ under varying conditions. The sensitivity of GDOES to carbon was found to be superior to EPMA. Profiles showed a C depletion zone under the oxide scale due to consumption of chromium carbides. Deeper into the alloy showed an increase in C due to carburization of the alloy. The extent of this carburization varied depending on the alloy and the exposure condition with the alloy 282 exposed at 700 °C and 300 bar of sCO₂ having the highest degree of carburization.

REFERENCES

- [1] H. Chen, D.Y. Goswami, E.K. Stefanakos, *Renewable and Sustainable Energy Reviews*, 14 (2010) 3059-3067.
- [2] V. Dostal, P. Hejzlar, M.J. Driscoll, *Nuclear Technology*, 154 (2017) 283-301.
- [3] B.D. Iverson, T.M. Conboy, J.J. Pasch, A.M. Kruizenga, *Applied Energy*, 111 (2013) 957-970.
- [4] I.G. Wright, B.A. Pint, J.P. Shingledecker, D. Thimsen, *Asme, Materials Considerations for Supercritical CO₂ Turbine Cycles*, 2013.
- [5] C.T. Fujii, R.A. Meussner, *Journal of the Electrochemical Society*, 114 (1967) 435-8.
- [6] T. Gheno, D. Monceau, J. Zhang, D.J. Young, *Corrosion Science*, 53 (2011) 2767-2777.
- [7] H.E. McCoy, *Corrosion*, 21 (1965) 84-94.
- [8] B.A. Pint, R.G. Brese, 4 - High-temperature materials, in: P. Friedman, R. Dennis (Eds.) *Fundamentals and Applications of Supercritical Carbon Dioxide (sCO₂) Based Power Cycles*, Woodhead Publishing, 2017, pp. 67-104.
- [9] D.J. Young, J. Zhang, C. Geers, M. Schutze, *Materials and Corrosion-Werkstoffe Und Korrosion*, 62 (2011) 7-28.
- [10] R.G. Brese, J.R. Keiser, B.A. Pint, *Oxidation of Metals*, 87 (2017) 631-642.
- [11] B.A. Pint, R.G. Brese, J.R. Keiser, *Effect of Pressure and Thermal Cycling on Compatibility in CO₂ for Concentrated Solar Power Applications*, *Proceedings of the ASME Turbo Expo: Turbine Technical Conference and Exposition*, Vol 9, 2017.
- [12] B.A. Pint, K.A. Unocic, R.G. Brese, J.R. Keiser, *Materials at High Temperatures*, In Press (2018).
- [13] T. Nelis, R. Payling, *Glow Discharge Optical Emission Spectroscopy: A Practical Guide*, The Royal Society of Chemistry, Cambridge, UK, 2003.
- [14] A. Jalowicka, W. Nowak, D.J. Young, V. Nischwitz, D. Naumenko, W.J. Quadackers, *Oxidation of Metals*, 83 (2015) 393-413.
- [15] N. Ghanbari, T. Waldmann, M. Kasper, P. Axmann, M. Wohlfahrt-Mehrens, *The Journal of Physical Chemistry C*, 120 (2016) 22225-22234.
- [16] A. Jalowicka, W.J. Nowak, D. Naumenko, W.J. Quadackers, *JOM*, 68 (2016) 2776-2785.
- [17] P. Huczowski, T. Olszewski, M. Schiek, B. Lutz, G.R. Holcomb, V. Shemet, W. Nowak, G.H. Meier, L. Singheiser, W.J. Quadackers, *Materials and Corrosion*, 65 (2014) 121-131.
- [18] E. Hejrani, D. Sebold, W.J. Nowak, G. Mauer, D. Naumenko, R. Vaßen, W.J. Quadackers, *Surface and Coatings Technology*, 313 (2017) 191-201.
- [19] M. Dumerval, S. Perrin, L. Marchetti, M. Tabarant, F. Jomard, Y. Wouters, *Corrosion Science*, 85 (2014) 251-257.
- [20] Y. Hatano, J. Shi, N. Yoshida, N. Futagami, Y. Oya, H. Nakamura, *Fusion Eng Des*, 87 (2012) 1091-1094.
- [21] S. Bouhieda, F. Rouillard, V. Barnier, K. Wolski, *Oxidation of Metals*, 80 (2013) 493-503.
- [22] S. Bouhieda, F. Rouillard, K. Wolski, *Materials at High Temperatures*, 29 (2012) 151-158.
- [23] T. Furukawa, F. Rouillard, *Progress in Nuclear Energy*, 82 (2015) 136-141.
- [24] L. Martinelli, C. Desgranges, F. Rouillard, K. Ginestar, M. Tabarant, K. Rousseau, *Corrosion Science*, 100 (2015) 253-266.
- [25] R. Pillai, A. Chyrkin, D. Grüner, W. Nowak, N. Zheng, A. Kliewe, W.J. Quadackers, *Surface and Coatings Technology*, 288 (2016) 15-24.
- [26] F. Rouillard, C. Cabet, K. Wolski, M. Pijolat, *Corrosion Science*, 51 (2009) 752-760.
- [27] F. Rouillard, T. Furukawa, *Corrosion Science*, 105 (2016) 120-132.
- [28] F. Rouillard, G. Moine, M. Tabarant, J.C. Ruiz, *Oxidation of Metals*, 77 (2011) 57-70.
- [29] S. Sarrade, D. Féron, F. Rouillard, S. Perrin, R. Robin, J.-C. Ruiz, H.-A. Turc, *The Journal of Supercritical Fluids*, 120 (2017) 335-344.
- [30] D. Young, P. Huczowski, T. Olszewski, T. Hüttel, L. Singheiser, W.J. Quadackers, *Corrosion Science*, 88 (2014) 161-169.
- [31] B.A. Pint, J.R. Keiser, in: *4th International Symposium on Supercritical CO₂ Power Cycles*, Pittsburgh, PA, 2014, pp. Paper #61.
- [32] B.A. Pint, J.R. Keiser, *JOM*, 67 (2015) 2615-2620.
- [33] B.A. Pint, P.F. Tortorelli, I.G. Wright, *Oxidation of Metals*, 58 (2002) 73-101.
- [34] W.J. Nowak, *J. Anal. At. Spectrom.*, 32 (2017) 1730-1738.
- [35] W.J. Quadackers, A. Elschner, W. Speier, H. Nickel, *Applied Surface Science*, 52 (1991) 271-287.

[36] J.P. Pfeifer, H. Holzbrecher, W.J. Quadackers, U. Breuer, W. Speier, *Fresenius Journal of Analytical Chemistry*, 346 (1993) 186-191.

[37] R.I. Olivares, D.J. Young, P. Marvig, W. Stein, *Oxidation of Metals*, 84 (2015) 585-606.

ACKNOWLEDGEMENTS

Research sponsored by the U. S. Department of Energy, Office of Fossil Energy, Crosscutting Research Program and Office and Office of Energy Efficiency and Renewable Energy, Solar Energy Technology Program (SunShot Initiative). Notice: This manuscript has been authored by UT-Battelle, LLC under Contract No. DE-AC05-00OR22725 with the U.S. Department of Energy. The United States Government retains and the publisher, by accepting the article for publication, acknowledges that the United States Government retains a non-exclusive, paid-up, irrevocable, world-wide license to publish or reproduce the published form of this manuscript, or allow others to do so, for United States Government purposes. The Department of Energy will provide public access to these results of federally sponsored research in accordance with the DOE Public Access Plan (<http://energy.gov/downloads/doe-public-access-plan>).